Synchronizing and Damping Torques Analysis of Nonlinear Voltage Regulators

Gurunath Gurrala, *Graduate Student Member, IEEE*, and Indraneel Sen

***Abstract*—This paper makes an attempt to assess the benefits of replacing a conventional generator excitation system (AVR + PSS) with a nonlinear voltage regulator using the concepts of synchronizing and damping torque components in a single machine infinite bus (SMIB) system. In recent years, there has been considerable interest in designing nonlinear excitation controllers, which are expected to give better dynamic performance over a wider range of system and operating conditions. The performance of these controllers is often justified by simulation studies on few test cases which may not adequately represent the diverse operating conditions of a typical power system. The performance of two such nonlinear controllers which are designed based on feedback linearization and include automatic voltage regulation with good dynamic performance have been analyzed using an SMIB model. Linearizing the nonlinear control laws along with the SMIB system equations, a Heffron Phillip's type of a model has been derived. Concepts of synchronizing and damping torque components have been used to show that such controllers can impair the small signal stability under certain operating conditions. This paper shows the possibility of negative damping contribution due to nonlinear voltage regulators and gives a new insight on understanding the physical impact of complex nonlinear control laws on power system dynamics.**

***Index Terms*—Feedback linearization, power system stabilizers, small-signal stability, transient stability.**

I. Introduction

In recent years, there has been considerable interest in designing nonlinear excitation controllers, which are expected to give better dynamic performance over a wider range of system and operating conditions. Several nonlinear control techniques such as feedback linearization, back stepping, variable structure control, synergy control theory, etc. [1]–[11] have been used for excitation system design. These controllers aim to replace the existing AVR + PSS structure, but the benefits of this replacement have not been properly quantified. This paper is an attempt in this direction, that is, to assess the merits and demerits of replacing the AVR + PSS structure with feedback linearization based voltage regulators in a single machine infinite bus system (SMIB).

Feedback linearization (FBL) technique has been widely used for generator excitation system design [2]–[4], [6], [7], [12]–[17]. Most of these nonlinear control designs based on FBL have formulated the excitation control problem as a regulator problem [17] and terminal voltage regulation was not considered in the design objective. This paper focuses on nonlinear voltage regulators because fast voltage regulation, though improves transient stability, has conflicting nature with the small signal stability [18] improvement. References [6] and [7] are two earlier designs which consider the excitation system design, with terminal voltage regulation as the objective. This paper analyzes these two nonlinear voltage regulators which are designed based on two different approaches of feedback linearization.

The terminal voltage of the machine is taken as output to derive the control law in [6] using Input-Output feedback linearization approach [19], for a single machine infinite bus system. In [7], the nonlinear control law is obtained by canceling the nonlinearities present in the derivative of active power equation of SMIB system. A robust linear controller is then designed by taking terminal voltage, speed and power as state variables. To analyze the small signal behavior of these voltage regulators over a wide operating range, the nonlinear control laws are linearized around an operating point. It has been observed that the linearized form of these nonlinear controllers has the same structure as that of a high gain static automatic voltage regulator but contains an additional positive feedback term from the speed deviations which we call as damping term because it acts like a stabilizing signal. Synchronizing and damping torque coefficients are derived from the linearized model of SMIB system including these nonlinear voltage regulators.

For the controller in [6], it is observed that under weak system conditions, the value of the damping term significantly reduces and the response becomes more oscillatory. It is also observed that the damping torque coefficient decreases with the increase in equivalent reactance as well as the system loading, and it becomes negative as the system becomes weak. It is shown that the effectiveness of this nonlinear AVR is usually better than that of a static AVR over a wide range but not as satisfactory as the performance of an AVR and PSS combination. However, for the controller in [7], the damping term and the damping torque coefficient increase with increase in equivalent reactance and loading as opposed to the controller in [6]. It has been shown that the nonlinear voltage regulator proposed in [7] can successfully replace the AVR+PSS structure for the SMIB test system considered over a wide range of operating conditions.

II. Modeling of Power System

IEEE Model 1.0 [20], [21] has been used to represent the synchronous generator in [6] and [7]. This results in a third-

Manuscript received December 25, 2009; revised January 01, 2010, January 05, 2010, April 11, 2010, and July 02, 2010; accepted August 16, 2010. Date of publication October 14, 2010; date of current version July 22, 2011. Paper no. TPWRS-01006-2009.

The authors are with the Department of Electrical Engineering, Indian Institute of Science, Bangalore 560012, India (e-mail: gurunath_gurrala@yahoo.co.in; sen@ee.iisc.ernet.in).

Digital Object Identifier 10.1109/TPWRS.2010.2070814

order dynamic model for the SMIB power system. The dynamic equations of SMIB system used in [6] and [7] are as follows:

$$\dot{\delta} = \omega_B S_m \tag{1}$$
$$\dot{S}_m = \frac{1}{2H}\{T_{\rm mech} - T_{\rm elec} - DS_m\} \tag{2}$$
$$\dot{E}'_q = \frac{1}{T'_{do}}\{-E'_q + (X_d - X'_d)i_d + E_{\rm fd}\} \tag{3}$$
$$T_{\rm elec} = E'_q i_q + (X'_d - X_q) i_d i_q. \tag{4}$$

The variables have standard meaning [21] and they are defined in the Appendix. Here the control variable is the field voltage $E_{\rm fd}$. The objective is to design a nonlinear control law for $E_{\rm fd}$ to get proper voltage regulation, i.e., terminal voltage $V_t \to V_{\rm ref}$ a prespecified voltage.

III. Nonlinear Voltage Regulator Design Proposed in [6]

In [6], the state variables for SMIB are defined as $x = \{\delta, S_m, E'_q\}$. Derivatives of the output V_t are taken successively until the control input $E_{\rm fd}$ appears in the equation. In this case, relative degree is one. Neglecting R_a, the terminal voltage V_t for an SMIB system is given by

$$V_t = \sqrt{\left[\left(\frac{X_q E_b \sin\delta}{X_e + X_q}\right)^2 + \left(\frac{X'_d E_b \cos\delta + X_e E'_q}{X_e + X'_d}\right)^2\right]} \tag{5}$$

taking derivative once we get

$$\dot{V}_t = \underbrace{\left\{\begin{array}{l}\frac{1}{\sqrt{V_t}}(V_d C_{11}\omega_B S_m \cos\delta - \dot{\delta} V_q C_{22} E_B \sin\delta) \\ +\frac{1}{\sqrt{V_t}}\frac{V_q C_{33}}{T'_{do}}(-E'_q + (X_d - X'_d) i_d)\end{array}\right\}}_{f(x)} + \underbrace{\left\{\frac{1}{\sqrt{V_t}}\frac{V_q C_{33}}{T'_{do}}\right\}}_{g(x)} E_{\rm fd} \tag{6}$$

where

$$C_{11} = \frac{X_q}{X_e + X_q}, \quad C_{22} = \frac{X'_d}{X_e + X'_d}$$
$$C_{33} = \frac{X_e}{X_e + X'_d}. \tag{7}$$

Equation (6) can be written in control affine form as

$$\dot{V}_t = f(x) + g(x)u. \tag{8}$$

Defining the tracking error as $e = V_t - V_{\rm ref}$, a fixed gain parameter $K_v > 0$ has been chosen so that the error dynamics $\dot{e} + K_v e = 0$ as $t \to \infty$. By solving the error dynamics equation, the following control law for field voltage $E_{\rm fd}$ has been obtained:

$$E_{\rm fd} = \frac{T'_{do}}{C_3 V_q}\left[\begin{array}{l}-K_v(V_t - V_{\rm ref})\sqrt{V_t} - (V_d C_{11}\cos\delta\omega_B \\ S_m E_b) + V_q C_{22} E_b \sin\delta\omega_B S_m\end{array}\right] + E'_q - (X_d - X'_d) i_d. \tag{9}$$

It is to be noted that K_v is the only gain parameter that needs to be tuned for improvement in the performance. This control law gives the necessary closed-loop control which, when applied, causes the output, terminal voltage, of the machine to behave linearly [6].

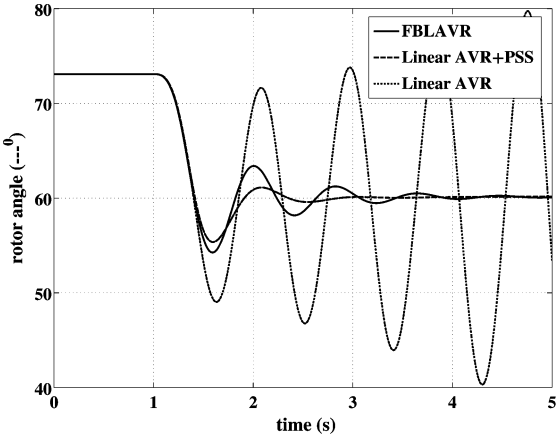

Fig. 1. δ response, 10% step change in $V_{\rm ref}$.

A. Simulation Results

The performance of the nonlinear AVR originally proposed in [6] has been extensively evaluated on an SMIB system used in [18] (machine data given in [18] for steam input is used here). Several operating conditions are created to test the performance of the proposed voltage regulator by varying X_e from 0.2 p.u. to 0.8 p.u. and P_g from 0.5 p.u. to 1 p.u. by keeping terminal voltage V_t, E_b at 1 p.u. The system performance is compared with a static AVR, with and without a power system stabilizer. Results of a few test cases are presented here. Here we consider $X_e \leq 0.3$ as strong system, $X_e \geq 0.6$ as weak system and $0.3 < X_e < 0.6$ as nominal system.

Fig. 1 shows the responses of the nominal SMIB system ($P_g + jQ_g = 1 + j0.2$ p.u., $V_t = 1$ p.u., $X_e = 0.4$ p.u.) in terms of the rotor angle δ for a 0.1 p.u. step change in $V_{\rm ref}$. The system is operated with (a) nonlinear AVR with $K_v = 20$ (FBLAVR), (b) static AVR (linear AVR) and (c) static AVR with PSS (linear AVR + PSS). The system is unstable with linear AVR alone. The system becomes stable with FBLAVR and the performance is comparable to that of a linear AVR + PSS controller. It has been observed that the terminal voltage response with $K_v = 20$ is almost close to the response obtained with linear AVR+PSS.

Fig. 2 shows the responses of the SMIB with the same operating conditions as above, following a 3ϕ fault at the transformer bus cleared after 50 ms by tripping one of the parallel

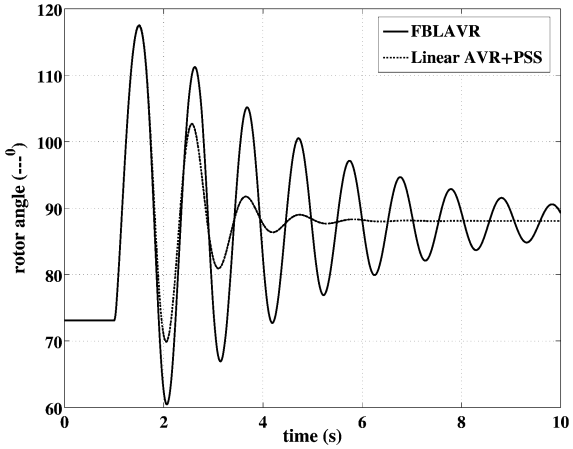

Fig. 2. δ response, 3ϕ fault at transformer bus, cleared by line tripping.

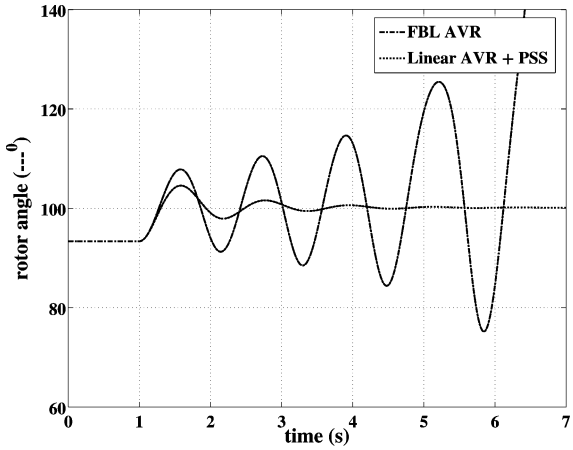

Fig. 3. δ response, 10% step change in T_m, weak system.

lines. After the fault is cleared, the system becomes weak with an equivalent external reactance $X_e = 0.7$ p.u. The system is more oscillatory with nonlinear AVR, whereas the performance of the linear AVR+PSS is much better. It has been observed that if the fault is cleared without line tripping, then the performance of this nonlinear AVR is much better than the linear AVR+PSS.

Fig. 3 shows the system responses for weak system ($P_g + jQ_g = 1 + j0.5$ p.u., $X_e = 0.8$ p.u, $V_t = 1$ p.u.). The responses are shown for a 10% step change in T_m. In this case, the response of the system is unstable with the nonlinear AVR.

From several simulations, it has been observed that the performance of the nonlinear AVR proposed in [6] is better than or comparable to the performance of the linear AVR + PSS only under nominal and strong system conditions. Its performance is poor even for small disturbances under heavy loading and weak system conditions. By seeing the nonlinear control law, it is not possible to explain the reasons for this poor performance. We make an attempt to understand this behavior using the concepts of synchronizing and damping torques analysis in the following sections.

B. Small-Signal Analysis

In order to understand the behavior of the nonlinear AVR at different operating conditions, the control law (9) is linearized using the conventional Taylor series approximation. Linearization of (9) gives

$$\Delta E_{\rm fd} = \frac{T'_{do}}{C_{33}V_{q0}} \left[\begin{array}{l} -K_v(\Delta V_t - \Delta V_{\rm ref})\sqrt{V_{\rm ref}} + \\ \left(\begin{array}{l} V_{q0}C_{22}E_b \sin\delta_0\omega_B \\ -V_{d0}C_{11}E_b \cos\delta_0\omega_B \end{array} \right) \Delta S_m \end{array} \right] + \Delta E'_q - (X_d - X'_d)\Delta i_d. \quad (10)$$

Linearizing V_t and i_d gives [21]

$$\Delta V_t = K_5\Delta\delta + K_6\Delta E'_q \quad (11)$$

$$\Delta i_d = C_1\Delta\delta + C_2\Delta E'_q \quad (12)$$

where

$$\begin{aligned} K_5 &= -\frac{X_q V_{d0}E_b\cos\delta_0}{(X_q + X_e)V_{\rm ref}} - \frac{X'_d V_{q0}E_b \sin\delta_0}{(X_e + X'_d)V_{t0}} \\ K_6 &= \frac{X_{te}}{X_e + X'_d}\frac{V_{q0}}{V_{t0}} \\ C_1 &= \frac{1}{\Lambda}[R_t V_{s0}\cos\delta_{s0} - (X'_q + X_t)V_{s0}\sin\delta_{s0}] \\ C_2 &= -\frac{1}{\Lambda}(X'_q + X_t) \\ \Lambda &= (X'_d + X_e)(X_q + X_e) + R_e^2 \end{aligned} \quad (13)$$

substituting (11) and (12) in (10) and rearranging the terms, one can arrive at (14) at the bottom of the next page, where $\Gamma_1 = V_{q0}E_b\omega_B C_{22}\sin\delta_0$ and $\Gamma_2 = V_{d0}E_b\omega_B C_{11}\cos\delta_0$, and this can be rewritten as

$$\Delta E_{\rm fd} = K_{\rm FBL}\left[\begin{array}{l} -G_5\Delta\delta - G_6\Delta E'_q + \Delta V_{\rm ref} \\ +G_D\Delta S_m \end{array} \right]. \quad (15)$$

Fig. 4 shows the block diagram representation of (15) which is same as the block diagram of a linear AVR [18] except for the additional component from speed deviations. From the block diagram, the output feedback linearization based AVR can be interpreted as a very fast exciter of negligible time constant and a high gain denoted by $K_{\rm FBL}$. It has two components negatively affecting the torque angle loop, one due to the deviations in rotor angle $\Delta\delta$ denoted by G_5 and the other due to the deviations in flux linkages $\Delta E'_q$ denoted by G_6. It also contains an additional component G_D due to the deviations in slip speed ΔS_m as shown with dashed circle in Fig. 4. This component G_D contributes positively to the torque angle loop just like a power system stabilizer. The sign of G_D indicates whether it deteriorates or aids the system damping. The equivalent of G_5, G_6 for linear AVR are denoted by K_5, K_6 which are standard Heffron-Phillip's parameters of an SMIB system.

Variations of parameters G_5, G_6, and equivalent exciter gain $K_{\rm FBL}$ are plotted by varying generator power P_g from 0.5 p.u. to 1.1 p.u. for various values of X_e by keeping the terminal voltage V_t and infinite bus voltage E_b constant at 1 p.u. Figs. 5 and 6 show the variations of K_5, G_5 and K_6, G_6, respectively, with P_g. Gain K_v of the nonlinear AVR is fixed at 20 so that the variations of G_5 and G_6 are almost the same as that of the linear

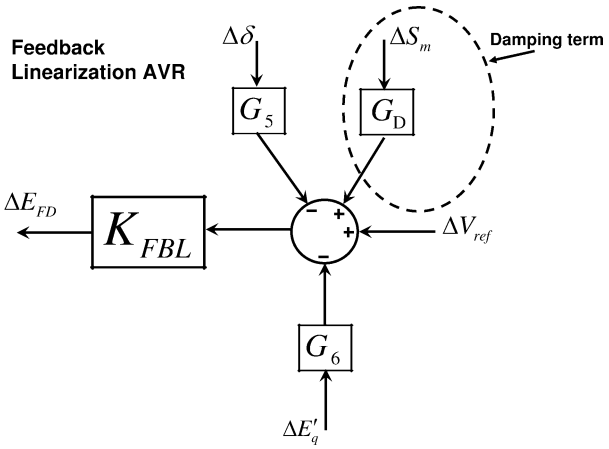

Fig. 4. Output feedback linearization based AVR.

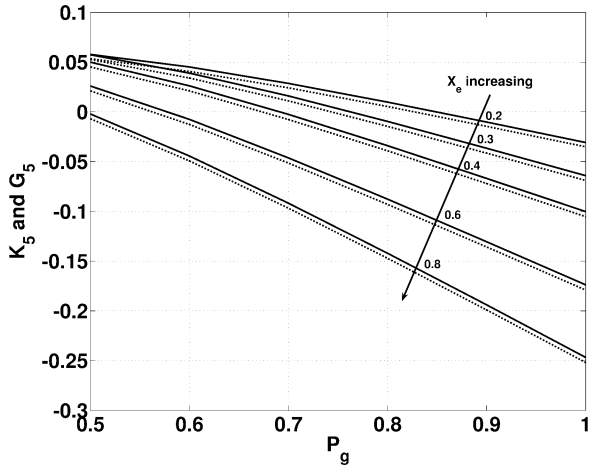

Fig. 5. Variation of G_5, K_5 with P_g for various values of X_e.

AVR parameters K_5 and K_6. For all foreseeable operating conditions, K_6 and G_6 are always positive. K_5 and G_5 can be however positive or negative. This has significant impact on system stability.

Fig. 7 shows the variation of the damping term G_D with P_g for different values of X_e. It can be inferred that the damping contribution due to G_D would reduce with increase in loading as well as system equivalent reactance. The nonlinear AVR, therefore, may not have good damping performance under heavy loading as well as weak transmission conditions.

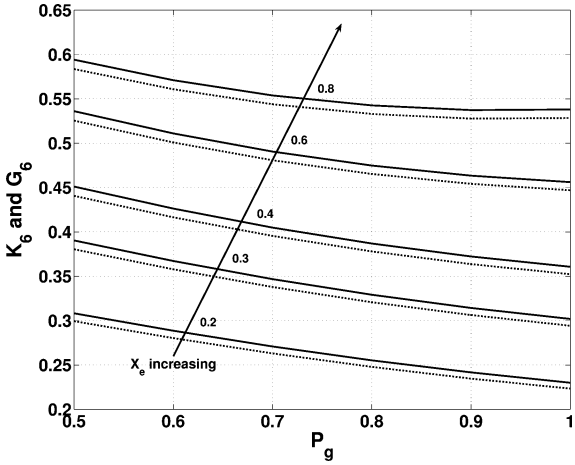

Fig. 6. Variation of G_6, K_6 with P_g for various values of X_e.

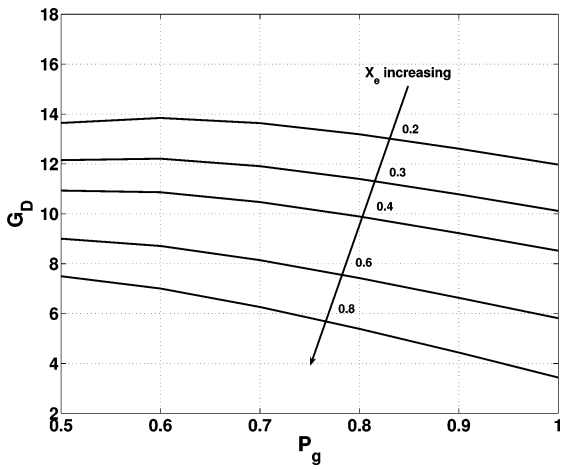

Fig. 7. Variation of G_D with P_g for various values of X_e.

Fig. 8 shows the variation of K_{FBL} with P_g and X_e. For X_e in the range of 0.2 to 0.8, K_{FBL} lies between 200 and 550 which falls in the usual range of the gain of linear AVR. It can be observed that as K_v appears in the denominator of G_D expression, increasing K_v reduces G_D. So the tuning parameter K_v can be varied only in a narrow range.

$$\Delta E_{\mathrm{fd}} = \frac{T'_{do}K_v\sqrt{V_{t0}}}{C_{33}V_{q0}} \times \left\{ \begin{array}{l} -\underbrace{\left[K_5 + \dfrac{(X_d - X'_d)\,V_{q0}C_{33}C_1}{T'_{do}K_v\sqrt{V_{t0}}}\right]}_{G_5}\Delta\delta - \underbrace{\left[-\dfrac{C_{33}V_{q0}}{T'_{do}K_v\sqrt{V_{t0}}} + \dfrac{(X_d - X'_d)V_{q0}C_{33}C_2}{T'_{do}K_v\sqrt{V_{t0}}} + K_6\right]}_{G_6}\Delta E'_q \\ +\Delta V_{\mathrm{ref}} + \underbrace{\dfrac{(\Gamma_2 - \Gamma_1)}{K_v\sqrt{V_{t0}}}}_{G_D}\Delta S_m \end{array} \right\} \quad (14)$$

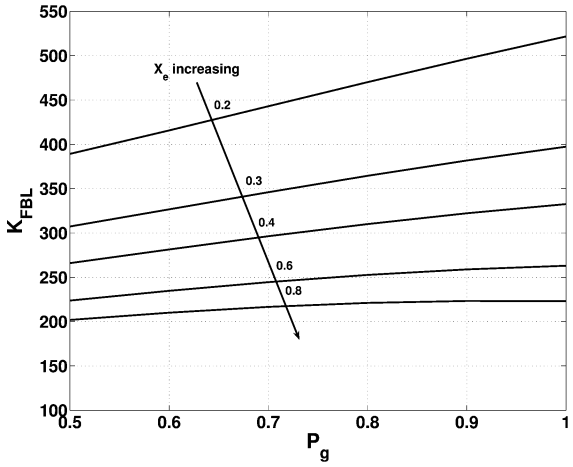

Fig. 8. Variation of K_{FBL} with P_g for various values of X_e.

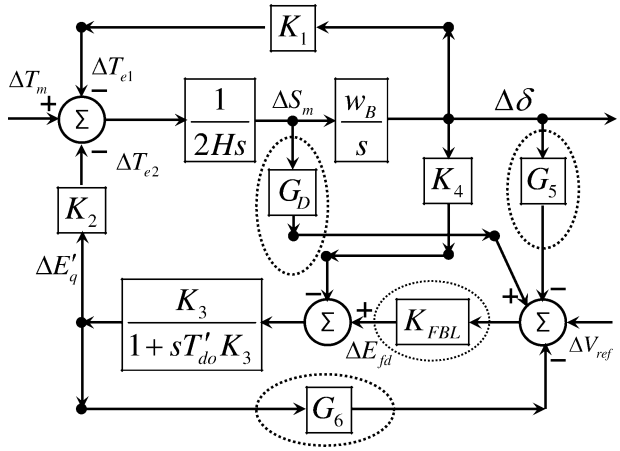

Fig. 9. Heffron Phillip's model including feedback linearization nonlinear AVR.

C. Synchronizing and Damping Torques Analysis

The block diagram of the SMIB system including nonlinear AVR is shown in Fig. 9. The component of electrical torque produced by voltage regulator action due to variations in rotor angle through E'_q can be expressed as

$$\Delta T_{e2} = \underbrace{\frac{K_2K_3[-K_4 - K_{\mathrm{FBL}}G_5]\Delta\delta}{1 + sT'_{do}K_3 + K_3K_{\mathrm{FBL}}G_6}}_{T_{\mathrm{elec1}}} + \underbrace{\frac{K_2K_3G_D\Delta S_m}{1 + sT'_{do}K_3 + K_3K_{\mathrm{FBL}}G_6}}_{T_{\mathrm{elec2}}}. \quad (16)$$

The first component T_{elec1} can be treated as the torque that would have been produced by a static AVR with a gain equal to K_{FBL} and low time constant, and this component is referred as linear part. The second component T_{elec2} can be considered as the torque produced by G_D due to the nonlinear AVR action, and this component is referred to as the nonlinear part. The system matrix with nonlinear voltage regulator can be obtained as

$$A_{\mathrm{FBL}} = \begin{bmatrix} 0 & \omega & 0 \\ \frac{-K_1}{2H} & \frac{-D}{2H} & \frac{-K_2}{2H} \\ \frac{-(K_4+K_{\mathrm{FBL}}G_5)}{T'_{do}} & \frac{(K_{\mathrm{FBL}}G_D)}{T'_{do}} & \frac{-\left(\frac{1}{K_3}+K_{\mathrm{FBL}}G_6\right)}{T'_{do}} \end{bmatrix}. \quad (17)$$

Substituting $s = a + jb$ (complex eigenvalue corresponding to the rotor mode of system matrix A_{FBL}) and $\Delta S_m = (s\Delta\delta)/(\omega_o)$ one can obtain the following expressions for synchronizing and damping torque coefficients [22]:

$$T_S = \underbrace{\mathrm{Re}\{T_{\mathrm{elec1}}\} + \left(\frac{-a}{b}\right)\mathrm{Im}\{T_{\mathrm{elec1}}\}}_{\text{Linear Part}} + \underbrace{\mathrm{Im}\{T_{\mathrm{elec2}}\}\left(-\frac{a^2}{b\omega_o} - \frac{b}{\omega_o}\right)}_{\text{Nonlinear Part}} \quad (18)$$

$$T_D = \underbrace{\mathrm{Im}\{T_{\mathrm{elec1}}\}\frac{\omega_o}{b}}_{\text{Linear Part}} + \underbrace{\mathrm{Re}\{T_{\mathrm{elec2}}\} + +\mathrm{Im}\{T_{\mathrm{elec2}}\}\frac{a}{b}}_{\text{Nonlinear Part}}. \quad (19)$$

Total synchronizing torque coefficient can be obtained by adding K_1 to (18). K_2 and K_4 are always positive and for the conceivable range of operating conditions, G_6 is positive as can be seen in Fig. 6. G_5, on the other hand, can be positive or negative depending upon the system condition as shown in Fig. 5. If $G_D = 0$, (18) and (19) reduce to the expression for the synchronizing and damping torque coefficients of a very fast linear voltage regulator with gain $K_A = K_{\mathrm{FBL}}$ and time constant $T_A = 0$. In this case, the following conclusions drawn in [18] are valid.

- When G_5 is negative, synchronizing torque coefficient T_S is positive, which is beneficial.
- when G_5 is positive, T_S is negative. This is of little consequence, as under such conditions, K_1 is large positive and the total synchronizing torque remains positive.
- The damping torque coefficient T_D is positive whenever G_5 is positive, but for a large number of cases, G_5 is negative and introduces negative damping.

Fig. 10 shows T_S due to linear part. Observe that T_S increases with increase in X_e and P_g. It can be understood that under strong system and light loading conditions, linear AVR fails due to lack of synchronizing torque. Fig. 11 shows the T_D due to linear part, which decreases with increase in X_e and P_g and eventually becomes negative when G_5 becomes negative. So linear AVR fails under heavy loading and weak system conditions due to negative damping torque. Hence, it is essential for any stabilizing controller to provide more damping torque under heavy loading and weak system conditions. If K_1 is not sufficiently large, the stabilizing controller should also provide more synchronizing torque under strong system and light loading conditions.

Figs. 12 and 13 show the variation of synchronizing and damping torque components contributed from the nonlinear part, i.e., due to the G_D component alone. Observe that both

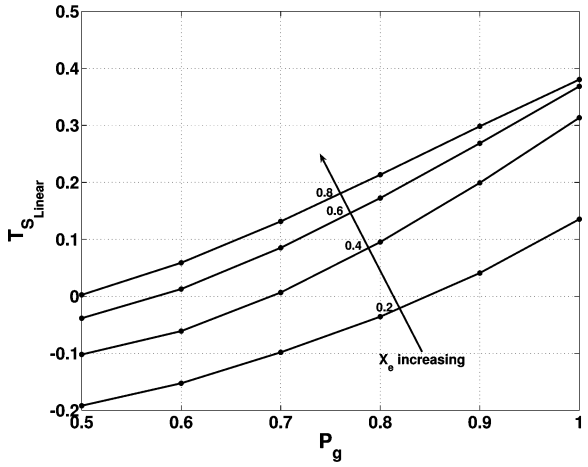

Fig. 10. T_S contribution due to linear part of controller proposed in [6].

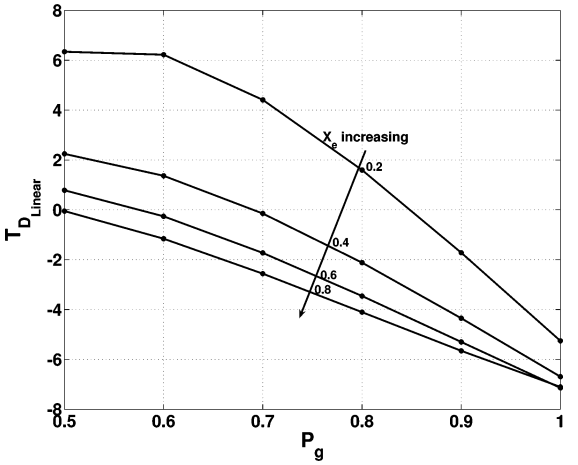

Fig. 11. T_D contribution due to linear part of controller proposed in [6].

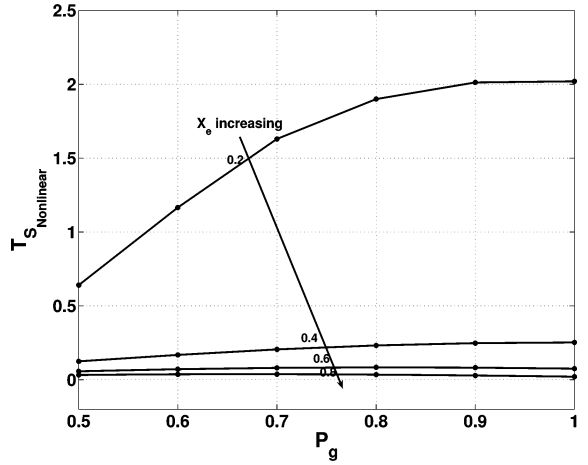

Fig. 12. T_S contribution due to nonlinear part of controller proposed in [6].

the torque components are positive over the whole range of operating and system conditions and they decrease with the increase in X_e. Their variation is not very significant with change in P_g except under strong system conditions. Higher

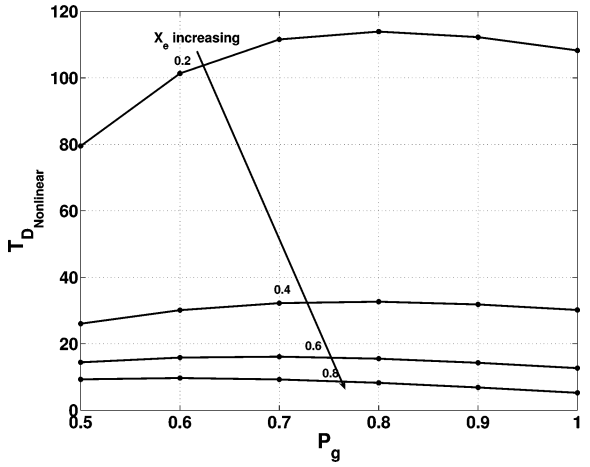

Fig. 13. T_D contribution due to nonlinear part of controller proposed in [6].

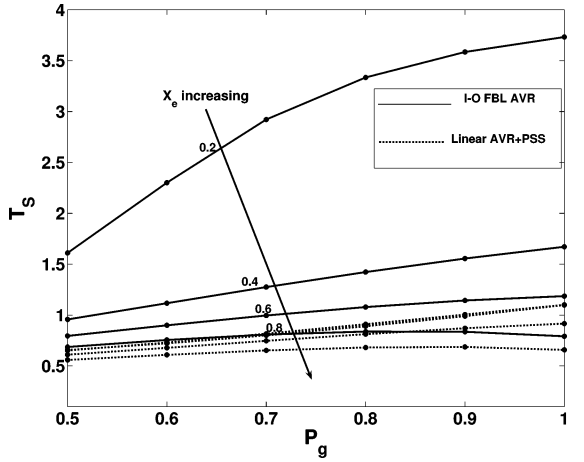

Fig. 14. Total T_S contribution of controller proposed in [6] and linear $\mathrm{AVR} + \mathrm{PSS}$.

values of T_S under strong system conditions is a desirable feature. The positive T_S values over the whole range indicates that the G_D component always aids the total T_S. However in Fig. 13, the damping torque under weak system conditions is very less and may not be sufficient to counteract the negative damping contribution from the linear part.

Fig. 14 shows the total synchronizing torque contribution from Input-Output FBLAVR and linear $\mathrm{AVR} + \mathrm{PSS}$. The behavior of this nonlinear AVR is similar to the linear $\mathrm{AVR} + \mathrm{PSS}$, i.e., T_S decreases with X_e. It can be observed that total T_S contribution from this nonlinear AVR is much higher than the linear $\mathrm{AVR}+\mathrm{PSS}$. Similarly, Fig. 15 shows the comparison of total T_D's. Here also the behavior is the same as linear $\mathrm{AVR} + \mathrm{PSS}$; however, the total T_D contribution of nonlinear AVR is not very satisfactory when compared with the linear $\mathrm{AVR} + \mathrm{PSS}$ except for $X_e = 0.2$ p.u. Observe that total T_D becomes negative for $X_e = 0.8$ p.u. and $P_g \geq 0.9$ p.u. These results are consistent with the simulation results. This explains the reason for the poor performance of this nonlinear AVR under heavy loading and weak system conditions.

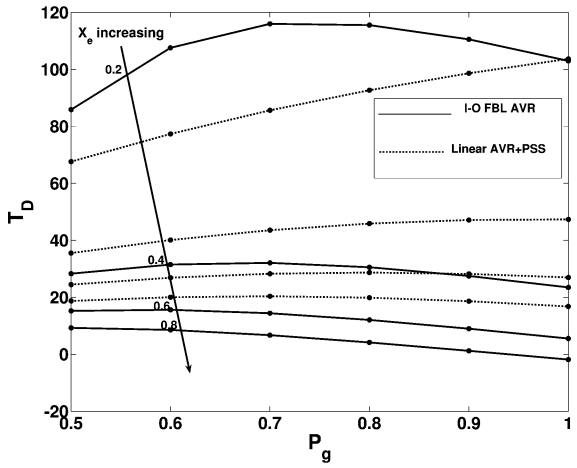

Fig. 15. Total T_D contribution of controller proposed in [6] and linear AVR + PSS.

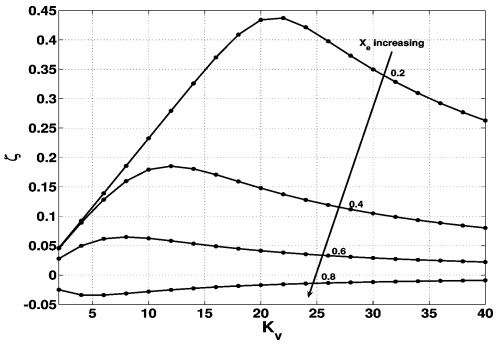

Fig. 16. Variation of damping factor ζ with K_v for various value of X_e.

Now we analyze the damping factor ζ obtained from the total T_S and T_D using the following expression [22]:

$$\zeta = \frac{1}{2}\frac{T_D}{\sqrt{2H\omega_B T_S}}. \tag{20}$$

Fig. 16 shows the variation of ζ with increase in K_v for various values of external reactance X_e by keeping the real power and terminal voltage constant. It can be observed that for each X_e value, the damping factor increases with increase in K_v, reaches maximum for some K_v, and then starts decreasing. The value of K_v at which maximum damping occurs decreases with increase in X_e. For the operating condition $P_g + jQ_g = 1 + j0.2$ p.u., $V_t = 1$ p.u., and $X_e = 0.4$ p.u., a maximum damping factor $\zeta_{\max} = 0.18525$ can be achieved with $K_v = 12$. Observe that ζ is not satisfactory ($\zeta < 0.15$) for $X_e \geq 0.6$ and becomes negative as $X_e \to 0.8$.

From the simulation results and the above observations, it can be inferred that the performance of the nonlinear regulator based on output feedback linearization proposed in [6] is always better than that of a linear AVR for the entire operating range. The performance of this nonlinear AVR is comparable to that of a linear AVR + PSS controller only over a limited range of operation. So the nonlinear AVR proposed in [6] may not be able to replace the linear AVR+PSS structure under high loads and weak system conditions because of the negative damping effect.

IV. Nonlinear Voltage Regulator Proposed in [7]

A new formulation for designing a voltage regulator for SMIB system was proposed in [7] using the third-order model for the synchronous machine. Nonlinear control law in [7] is derived so as to cancel the nonlinearities in the derivative of the generator active power output. A robust controller is then designed for the new input taking V_t, S_m, and P_g as state variables. This is a full state feedback controller. The active power output of SMIB system is given by

$$P_g = \frac{E'_q E_b \sin\delta}{X_q + X_e}. \tag{21}$$

Taking derivative of P_g

$$\dot{P}_g = \frac{E_b \sin\delta}{X_q + X_e}\dot{E}'_q + \frac{E'_q E_b \cos\delta}{X_q + X_e}\dot{\delta} \tag{22}$$

after rearrangement, one can get

$$\dot{P}_g = -\frac{P_g}{T'_{do}} + \frac{1}{T'_{do}}\left\{\begin{array}{l} I_q[E_{\rm fd} + (X_d - X_q)I_d] \\ +T'_{do}\frac{E'_q E_b \cos\delta}{X_q + X_e}\omega_B S_m \end{array}\right\} \tag{23}$$

define a new input V_f as

$$V_f = I_q[E_{\rm fd} + (X_d - X_q)I_d] + T'_{do}\frac{E'_q E_b \cos\delta}{X_q + X_e}\omega_B S_m - P_m. \tag{24}$$

This input cancels the nonlinearities in $\dot{P}_g$ and makes it linear as follows:

$$\dot{P}_g = -\frac{P_g - P_m}{T'_{do}} + \frac{1}{T'_{do}}V_f. \tag{25}$$

Solving for field voltage $E_{\rm fd}$, one can get the nonlinear control law as

$$E_{\rm fd} = \frac{1}{I_q}\left[V_f - T'_{do}\frac{E'_q E_b \cos\delta}{X_q + X_e}\omega_B S_m + P_m\right] - (X_d - X_q)I_d. \tag{26}$$

New input V_f is designed by robust control technique. The following state–space equation has been used for this, which is formulated by taking the derivative of terminal voltage

$$\dot{x} = Ax + BV_f \tag{27}$$

where

$$A = \begin{bmatrix} 0 & f_1 & -f_2 \\ 0 & \frac{-D}{2H} & -\frac{\omega_B}{2H} \\ 0 & 0 & -\frac{1}{T'_{do}} \end{bmatrix}; \quad B = \begin{bmatrix} \frac{f_2}{T'_{do}} & 0 & \frac{1}{T'_{do}} \end{bmatrix}$$

$$f_1 = \frac{P_g^2 X_e^2 \cos\delta}{V_t E_b^2 \sin^3\delta} - \frac{X_e X_q P_g}{V_t(X_q + X_e)\sin^2\delta}$$

$$f_2 = \frac{P_g X_e^2}{V_t E_b^2 \sin^2\delta} + \frac{X_e X_q \cos\delta}{V_t(X_q + X_e)\sin\delta}.$$

The final form of V_f is as follows, which is obtained by solving an algebraic Riccati equation whose details are skipped here [7]:

$$V_f = -K_V \Delta V_t - K_w \omega_B \Delta S_m - K_p \Delta P_g. \tag{28}$$

The final control law for voltage regulation is given by

$$E_{\text{fd}} = \frac{1}{I_q} \begin{bmatrix} -K_V \Delta V_t - K_w \omega_B \Delta S_m - K_p \Delta P_g \\ -T'_{do} \frac{E'_q E_b \cos\delta}{X_q + X_e} \omega_B S_m + P_m \end{bmatrix} - (X_d - X_q) I_d. \tag{29}$$

Note that in [7], the expression $(E'_q E_b \cos\delta)/(X_q + X_e)$ is replaced with $(Q_g + (E_b^2)/(X_q + X_e))$ to eliminate δ measurement. However, this is valid only if $V_t = E_b$. So we have not used this change in the present analysis.

A. Small Signal Analysis

The nonlinear control law (29) is linearized around an operating condition to analyze the small-signal behavior. Linearizing (29) gives (30) at the bottom of the page. Note that in per unit quantities, $\Delta P_g = \Delta T_e$ (torque). The linearized equations of ΔP_g and ΔI_q are as follows [21]:

$$\Delta P_g = K_1 \Delta\delta + K_2 \Delta E'_q \tag{31}$$

$$\Delta I_q = C_3 \Delta\delta + C_4 \Delta E'_q \tag{32}$$

where

$$C_3 = \frac{1}{\Lambda}[(X'_d + X_e) E_b \cos\delta_o + R_e E_b \sin\delta_o]$$
$$C_4 = \frac{R_e}{\Lambda}. \tag{33}$$

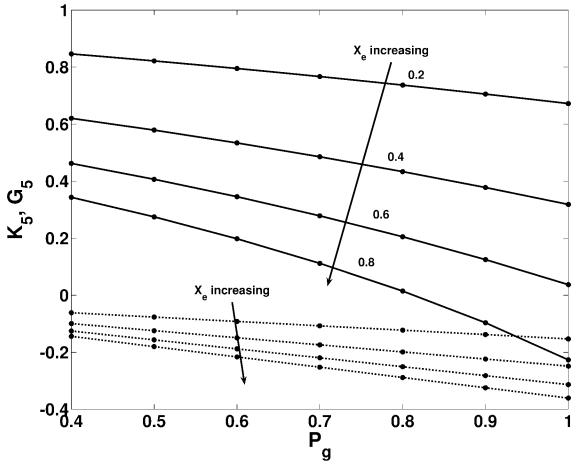

Fig. 17. Variation of G_5, K_5 with P_g for the nonlinear AVR proposed in [7].

Substituting (12), (32), (11) and (31) in (30), one can get (34) at the bottom of the page. Observe that this equation is again in the same form as (15) and the block diagram of this nonlinear controller is also the same as the previous case. Any controller, whether linear or nonlinear, should have a feedback from speed to produce a damping torque on the system. So one can generalize the block diagram shown in Fig. 4 for any nonlinear voltage regulator. Synchronizing and damping torques analysis can be applied to understand the small-signal behavior over a wide range of operating and system conditions. Here the analysis is carried out using the same SMIB system used in [7], and the comparison is made with the static AVR + PSS whose parameters are given in [7].

Fig. 17 shows the variation of K_5 and G_5 with P_g for various values of X_e. The dotted lines correspond to K_5 and solid lines correspond to G_5. Observe that the G_5 variation is positive for most of the operating conditions and it is far away from K_5

$$\Delta E_{\text{fd}} = \frac{1}{I_{qo}} \begin{bmatrix} -K_V \Delta V_t + K_V \Delta V_{\text{ref}} - K_w \omega_B \Delta S_m - K_p \Delta P_g \\ -T'_{do} \frac{E'_{qo} E_b \cos\delta_o}{X_q + X_e} \omega_B \Delta S_m - E'_{qo} \Delta I_q \end{bmatrix} - (X_d - X_q) \Delta I_d \tag{30}$$

$$\Delta E_{\text{fd}} = \frac{K_V}{I_{qo}} \left\{ \begin{array}{l} -\underbrace{\left[K_5 + \frac{K_p}{K_V} K_1 + \frac{C_3 E'_{qo}}{K_V} + \frac{(X_d - X_q) C_1 I_{qo}}{K_V} \right]}_{G_5} \Delta\delta \\ +\underbrace{\left[-\frac{K_w}{K_V} - T'_{do} \frac{E'_{qo} E_b \cos\delta_o}{(X_q + X_e) K_V} \right]}_{G_D} \omega_B \Delta S_m \\ -\underbrace{\left[K_6 + \frac{K_p}{K_V} K_2 + \frac{C_4 E'_{qo}}{K_V} + \frac{(X_d - X_q) C_2 I_{qo}}{K_V} \right]}_{G_6} \Delta E'_q \\ +\Delta V_{\text{ref}} \end{array} \right\} \tag{34}$$

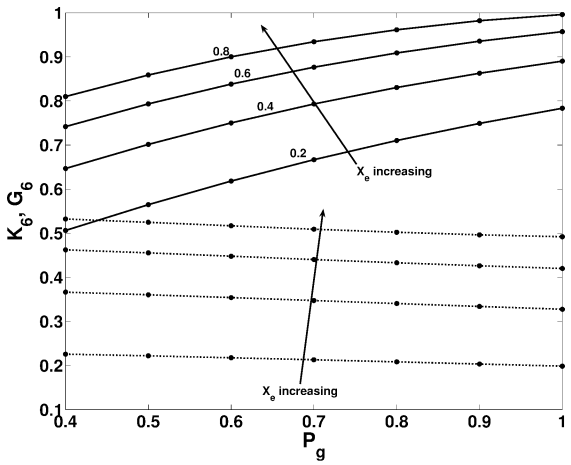

Fig. 18. Variation of G_6, K_6 with P_g for the nonlinear AVR proposed in [7].

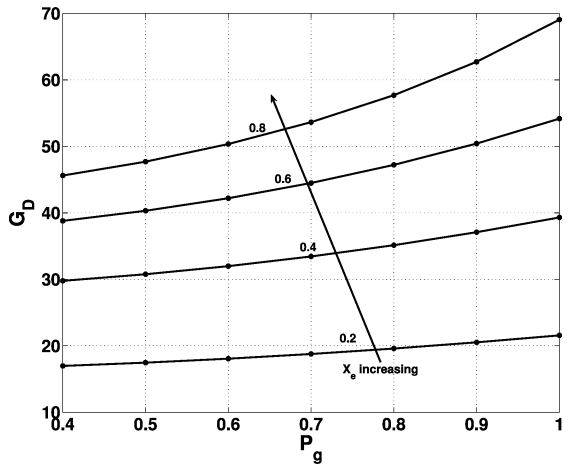

Fig. 19. Variation of G_D with P_g for nonlinear AVR proposed in [7].

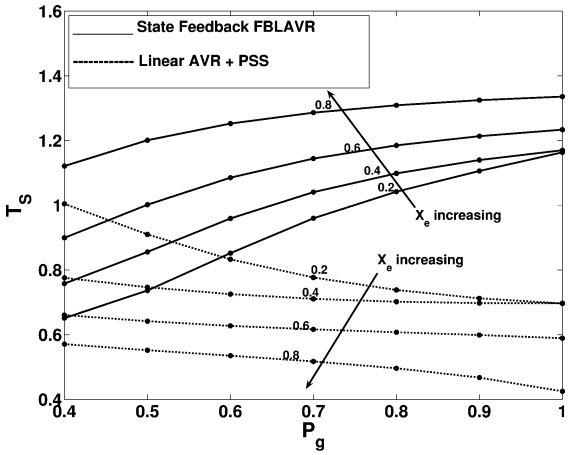

Fig. 20. Total T_S contribution of controller proposed in [7] and linear AVR + PSS.

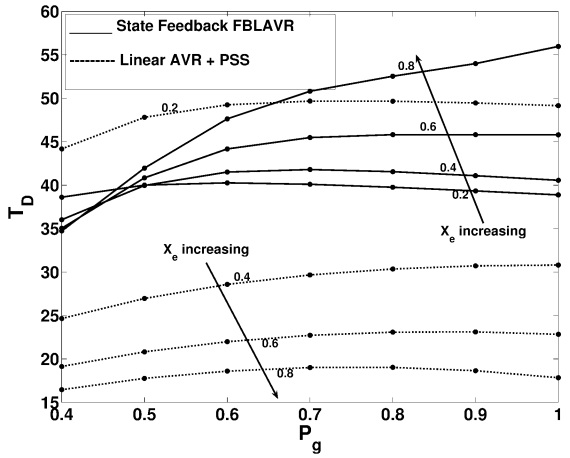

Fig. 21. Total T_D contribution of controller proposed in [7] and linear AVR + PSS.

variation. One may expect reduction of T_S due to positive G_5 but this rescues the negative damping effect. One can observe similar behavior in the variation of G_6 when compared to K_6 as shown in Fig. 18. Though the increase in G_6 increases damping torque, it is not very significant. It has been observed that the variation of equivalent exciter gain K_{FBL} is not very significant with change in X_e but it decreases considerably from 110 to 50 with increase in P_g. Reduction of the gain reduces T_S [22].

Fig. 19 shows the variation of G_D. Observe that the variation of G_D with this nonlinear AVR increases with increase in X_e and P_g which is exactly opposite to the controller studied in the previous section. This is a desirable feature as the linear AVR + PSS generally fails under weak system condition and heavy loading. So one can expect good damping torque contribution from this nonlinear AVR.

B. Synchronizing and Damping Torques Analysis

For this controller, also the T_S and T_D are computed at the rotor mode eigenvalues obtained from the system matrix A_{FBL} using (18) and (19) by varying P_g and X_e. Here, also the contribution due to linear part and nonlinear part are separately analyzed but the figures are not shown here due to space limitations.

It has been observed that for this controller, also the variation of T_S and T_D due to linear part are consistent with the conclusions of [18]. However, T_S and T_D due to nonlinear part are positive over the whole operating range and they increase with increase in X_e and loading, which is just opposite to the behavior of the previous controller. This is an essential feature expected from a stabilizing controller, and thus, this controller is expected to provide good damping to the system over a wide range of operating and system conditions. Though [7] claims that this controller is robust within $X_L + X_T \leq X_e \leq 2X_L + X_T$, this analysis shows that the controller is robust in much wider range $0.2 \leq X_e \leq 0.8$, which is the usual range one may expect for the external reactance.

Figs. 20 and 21 show the comparison of the total T_S, T_D produced by this nonlinear controller with the total T_S, T_D produced by linear AVR+PSS given in [7]. The solid lines referred as state feedback FBLAVR corresponds to the nonlinear AVR and dotted lines correspond to the linear AVR + PSS. Observe that the T_S, T_D variations of this nonlinear AVR are exactly opposite to the variation of linear AVR+PSS. The total T_D contribution increases with increase in loading and X_e. Fig. 22 shows the variation of damping factor ζ with P_g for various values of X_e. For this controller, ζ is not plotted against the gains of

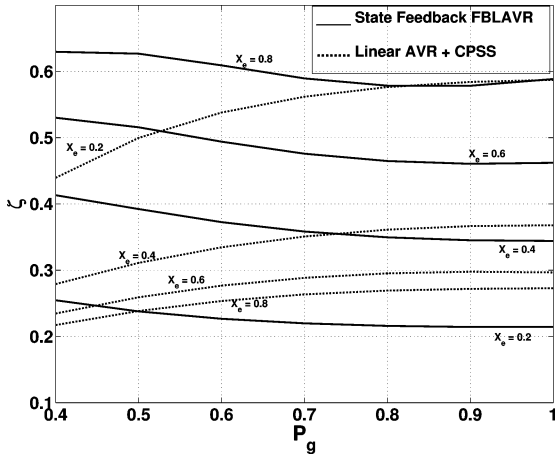

Fig. 22. Variation of damping factor ζ with P_g for various value of X_e.

the controller as the gains are not tunable arbitrarily and they need to be obtained by solving algebraic equation. It can be observed that the damping ratio increases with increase in X_e and remains constant with loading above 0.7 p.u. Hence, one can expect better small signal performance due to the nonlinear AVR proposed in [7] under weak system and heavy loading conditions where the linear $\mathrm{AVR}+\mathrm{PSS}$ generally fails. These observations have been verified by extensive simulation studies.

This analysis gives an insight that the controller proposed in [7] overcomes all the drawbacks of a linear $\mathrm{AVR}+\mathrm{PSS}$ and can replace the conventional $\mathrm{AVR}+\mathrm{PSS}$ structure over the entire range of operating and system conditions for the SMIB test system considered. The results of the controller proposed in [6] show the need for small signal performance assessment of the nonlinear controllers. As the synchronizing and damping torques approach is more general, it can be possibly extended to multimachine systems as well. However, due to the presence of multimodal oscillations in such systems, the validity of the proposed approach of analysis needs to be established by appropriate simulation studies on real interconnected systems.

V. Conclusion

This paper analyzes the performance of two different feedback linearization based nonlinear voltage regulators proposed in [6] and [7] for a single machine infinite bus system. The synchronizing and damping torques analysis has been shown to be effective in quantifying the merits and demerits of replacing the existing $\mathrm{AVR}+\mathrm{PSS}$ structure with nonlinear voltage regulators in an SMIB system over a wide range of system and operating conditions. This paper gives a new insight on understanding the physical impact of complex nonlinear control laws on power system dynamics. It has been shown that the performance of the nonlinear AVR proposed in [6] is always better than that of a conventional static AVR system. Its performance is also comparable with that of a static $\mathrm{AVR}+\mathrm{PSS}$ over a limited range of operating conditions. The small signal stability performance is however poor, especially under weak system conditions and cannot replace the AVR+PSS structure for the entire operating range. In the case of nonlinear voltage regulator proposed in [7], the synchronizing and damping torques analysis has shown that the performance of this regulator is much better than that of a conventional $\mathrm{AVR}+\mathrm{PSS}$ over the entire range of operating and system conditions. This shows the necessity of analyzing small signal performance of nonlinear voltage regulators. The proposed method of analysis based on computation of synchronizing and damping torques is thus useful in analyzing the small signal performance of nonlinear voltage regulators in single machine infinite bus systems.

Appendix
Variables Definitions

ω, ω_B	Angular speed and base speed.
δ	Rotor angle.
S_m	Slip speed $= (\omega - \omega_B)/(\omega_B)$.
T_{mech}, T_{elec}	Mechanical and electrical torques, respectively.
D	Damping coefficient.
E'_q	Transient induced voltage due to field flux-linkages.
i_d, i_q	d-axis and q-axis components of stator current.
T'_{do}	d-axis time constant.
X_d, X'_d	d-axis reactances,
X_q, X'_q	q-axis reactances.
E_{fd}	Field voltage.
$V_t \angle \theta$	Voltage measured at the generator terminal.
V_{ref}	Reference voltage.
V_{pss}	PSS input.
R_a	Armature resistance,
X_t, X_L	Transformer and transmission line reactances.
V_d, V_q	d and q-axis components of terminal voltage.
K_A, T_A	Gain and time constants of static excitation system.
H	Inertia constant of machine.
P_g, Q_g	Real and reactive power.
E_b	Infinite bus voltage.

References

[1] J. W. Chapman, M. D. Ilic, C. A. King, L. Eng, and H. Kaufman, "Stabilizing a multi machine power system via decentralized feedback linearizing excitation control," *IEEE Trans. Power Syst.*, vol. 8, no. 3, pp. 830–839, Aug. 1993.

[2] Q. Lu and Y. Sun, "Nonlinear stabilizing control of multi machine systems," *IEEE Trans. Power Syst.*, vol. 4, no. 1, pp. 236–241, Feb. 1989.

[3] L. Gao, L. Chen, Y. Fan, and H. Ma, "A nonlinear control design for power systems," *Automatica*, vol. 28, pp. 975–979, 1992.

[4] Y. Wang, D. J. Hill, R. H. Middleton, and L. Gao, "Transient stability enhancement and voltage regulation of power systems," *IEEE Trans. Power Syst.*, vol. 8, no. 2, pp. 620–627, May 1993.

[5] Y. Cao and O. P. Malik, "A nonlinear variable structure stabilizer for power system stability," *IEEE Trans. Energy Convers.*, vol. 9, no. 3, pp. 489–495, Sep. 1994.

[6] F. K. Mak, "Design of nonlinear generator excitors using differential geometric control theories," in *Proc. 31st IEEE Conf. Decision Control*, Tuscon, AZ, 1992, pp. 1149–1153.
[7] C. Zhu, R. Zhou, and Y. Wang, "A new nonlinear voltage controller for power systems," *Int. J. Elect. Power Energy Syst.*, vol. 19, pp. 19–27, 1997.
[8] G. J. Li, T. Lie, C. B. Soh, and G. H. Yang, "Decentralised nonlinear H_∞ control for stability enhancement in power systems," *Proc. Inst. Elect. Eng., Gen., Transm., Distrib.*, vol. 146, no. 1, pp. 19–24, Jan. 1999.
[9] B. K. Kumar, S. Singh, and S. Srivastava, "A decentralized nonlinear feedback controller with prescribed degree of stability for damping power system oscillations," *Elect. Power Syst. Res.*, vol. 77, no. 3–4, pp. 204–211, Mar. 2007.
[10] Z. Jiang, "Design of a nonlinear power system stabilizer using synergetic control theory," *Elect. Power Syst. Res.*, vol. 79, pp. 855–862, 2009.
[11] B. Wang and Z. Mao, "Nonlinear variable structure excitation and steam valving controllers for power system stability," *J. Control Theory Appl.*, vol. 7, no. 1, pp. 97–102, 2009.
[12] R. Marino, "An example of a nonlinear regulator," *IEEE Trans. Autom. Control*, vol. AC-29, no. 3, pp. 276–279, Mar. 1984.
[13] M. Ilic and F. K. Mak, "A new class of fast nonlinear voltage controllers and their impact on improved transmission capacity," in *Proc. 1989 American Control Conf.*, 1989, vol. 2, pp. 1246–1251.
[14] J. W. Chapman, M. D. Ilic, C. A. King, L. Eng, and H. Kaufman, "Stabilizing a multimachine power system via decentralized feedback linearizing excitation control," *IEEE Trans. Power Syst.*, vol. 8, no. 3, pp. 830–839, Aug. 1993.
[15] C. A. King, J. W. Chapman, and M. D. Ilic, "Feedback linearizing excitation control on a full-scale power system model," *IEEE Trans. Power Syst.*, vol. 9, no. 2, pp. 1102–1109, May 1994.
[16] Y. Guo, D. J. Hill, and Y. Wang, "Global transient stability and voltage regulation for power systems," *IEEE Trans. Power Syst.*, vol. 16, no. 4, pp. 678–688, Nov. 2001.
[17] D. J. Hill, Y. Guo, M. Larsson, and Y. Wang, *Global Control of Complex Power Systems*. Berlin/Heidelberg, Germany: Springer, 2004, vol. 293, Lecture Notes in Control and Information Sciences.
[18] F. P. Demello and C. Concordia, "Concepts of synchronous machine stability as affected by excitation control," *IEEE Trans. Power App. Syst.*, vol. PAS-88, no. 4, pp. 316–329, Apr. 1969.
[19] J. J. E. Slotine and W. Li, *Applied Nonlinear Control*. Englewood Cliffs, NJ: Prentice-Hall, 1991.
[20] IEEE Task Force, "Current usage and suggested practices in power system stability simulations for synchronous machines," *IEEE Trans. Energy Convers.*, vol. EC-1, no. 1, pp. 77–93, Mar. 1986.
[21] K. R. Padiyar, *Power System Dynamics Stability and Control*. New York: Wiley/Interline, 1996.
[22] P. S. Kundur, *Power System Stability and Control*. New York: McGraw-Hill, 1994.

Gurunath Gurrala (GS'09) received the B.Tech degree in electrical and electronics engineering from S.V.H. College of Engineering, Nagarjuna University, Guntar, India, in 2001 and the M.Tech degree in electrical power systems from J.N.T.U. College of Engineering, Anantapur, India, in 2003. He is currently pursuing the Ph.D. at the Indian Institute of Science, Bangalore, India.

He worked as an Assistant Professor in Anil Neerukonda Institute of Technology and Sciences (ANITS), Visakhapatnam, India, from 2003 to 2005. His research interests include power system stability, grid integration of renewables, flexible AC transmission systems, artificial intelligence applications to power systems, and nonlinear and adaptive control of power systems.

Indraneel Sen received the Ph.D. degree from IISc, Bangalore, India, in 1981. He is currently an Associate Professor in the Department of Electrical Engineering at the Indian Institute of Science, Bangalore. His research interests include power system stability, adaptive control, and energy management systems.